https://doi.org/10.5194/egusphere-2023-1347
Preprint. Discussion started: 30 August 2023
© Author(s) 2023. CC BY 4.0 License.

Direct Estimation of Global Anthropogenic CO_2 Emissions Using Satellite Data

Jia He[1], Bo Huang[1,2,3]

[1]Department of Geography and Resource Management, The Chinese University of Hong Kong, Hong Kong, China
[2]Institute of Space and Earth Information Science, The Chinese University of Hong Kong, Hong Kong, China
[3]Shenzhen Research Institute, The Chinese University of Hong Kong, Shenzhen, Guangdong, China

Correspondence to: Bo Huang(bohuang@hku.hk)

Abstract. Reliable statistics on anthropogenic CO_2 emissions are fundamental for carbon cycle and climate change research. Satellite observations offer a potential objective and efficient alternative to the current self-reporting mechanism. However, the current satellite projects provide only column-averaged CO_2 amount (XCO_2) data. This paper proposes a direct estimation method based on satellite-based CO_2 column amount, different from the conventional "top-down" approaches, which usually adopt satellite-observed data as an indicator to disaggregate consumption statistics. Here, the monthly CO_2 emissions from 2010 to 2019 are estimated globally using CO_2 data retrieved from the Greenhouse Gases Observing Satellite. The geographically and temporally weighted regression model is adopted to account for local spatial and temporal variability. The enhanced XCO_2 data and the local wind speed, vertical velocity, air temperature, water vapor concentration, and fire emissions are included in the estimation process. The validation results of the newly derived CO_2 emissions strongly agree with the Open-source Data Inventory for Anthropogenic CO_2 data ($R^2 = 0.929$). This high global consistency demonstrates the great potential of direct estimation from satellites, with improved frequency and a broader coverage range.

1 Introduction

Carbon dioxide (CO_2) is one of the most important greenhouse gases contributing to Earth's radiative budget and climate change (Pachauri et al., 2015; Solomon et al., 2007, 2009). It has a long lifetime in the atmosphere and is uniformly distributed with other atmospheric components. Over the past few decades, the concentration of atmospheric CO_2 has risen steadily owing to human activities, particularly those resulting in fossil fuel emissions (Friedlingstein et al., 2021, 2019; Schneising et al., 2011). To promote a sustainable low-carbon economy, the Paris Agreement of the UN Framework Convention on Climate Change (UNFCCC) proposed greenhouse gas mitigation pledges for countries to contribute to carbon emission reduction. A reliable and accurate monitoring system for anthropogenic greenhouse gas emissions and removal is urgently required to enable various governments to assess the mitigation progress.

https://doi.org/10.5194/egusphere-2023-1347
Preprint. Discussion started: 30 August 2023
© Author(s) 2023. CC BY 4.0 License.

Observations from ground-based stations provide valuable insights into the growth rate and trend of atmospheric CO_2 (Solomon et al., 2009; O'Neill et al., 2012); however, the observation network is too sparse to enable the accurate inference of carbon emissions on a global scale. CO_2 inventories are fundamental for managing CO_2 emissions at multiple scales, investigating emissions sources, and analyzing development trends (Le Quéré et al., 2020; Liu et al., 2020). The correlations between CO_2 emissions and population density (Olivier et al., 2005), night light (Oda and Maksyutov, 2011), and other geographical information such as point source locations and road networks (Crippa et al., 2022) are considered in the construction of gridded emissions maps. However, the capacity and quality of the self-reported datasets vary across and within countries (Xu, 2020), which makes it difficult to guarantee the accuracy and consistency of the estimated results.

Space-based remote sensing observations provide complementary measurements from the existing surface-based greenhouse gas monitoring network over the globe (Crowell et al., 2019). Several satellite missions have been developed to obtain the column-averaged CO_2 dry air mole fraction (XCO_2) as an indicator for the vertically integrated CO_2 in an entire atmospheric column (Cogan et al., 2012; Yang et al., 2021). The cluster analysis of XCO_2 anomalies (ΔXCO_2) extracted from the Orbiting Carbon Observatory-2 (OCO-2) confirmed the positive correlation between CO_2 and emission inventories, allowing for the isolation of low-emission areas (Hakkarainen et al., 2016). However, this research was greatly limited, as it did not include a quantitative estimation of CO_2 emissions. Pan et al. (2021) proposed a multiple linear regression model to estimate CO_2 emissions from OCO-2 XCO_2 data in China, and validation against the Open-source Data Inventory for Anthropogenic CO_2 (ODIAC) showed that the overall R^2 was 0.486. The discrepancies between the modeled data and ODIAC indicate that the model's estimation did not fully explain the CO_2 emissions. Yang et al. (2019) proposed a general regression neural network model to estimate anthropogenic CO_2 emissions using ΔXCO_2 anomalies derived from the Greenhouse gases Observing SATellite (GOSAT) in China, with an R^2 of 0.65. Unfortunately, the annual estimation frequency considerably restricts the applicability of the model for the global characterization of carbon emissions.

In this study, a novel approach for the direct estimation of global anthropogenic emissions with multi-year XCO_2 data from GOSAT is proposed. Unlike previous studies that usually employed auxiliary data, emission inventories, or other proxies to estimate CO_2 emissions, this study utilized the geographically and temporally weighted regression (GTWR) model to estimate anthropogenic emissions from satellite-based CO_2 columns. The GTWR model simultaneously incorporates temporal information into spatial variability through a spatial-temporal weighting mechanism, providing a robust and complementary estimation of CO_2 emissions using enhanced XCO_2 data retrieved from satellite images. The primary objectives of this study are threefold: to develop an independent method to estimate CO_2 emissions directly from satellite-based measurement; to adopt the neat space-time statistical model GTWR in the estimation process; and to validate and analyze the applicability of the estimated results for future environmental research.

https://doi.org/10.5194/egusphere-2023-1347
Preprint. Discussion started: 30 August 2023
© Author(s) 2023. CC BY 4.0 License.

2 Data

2.1 XCO_2 and local enhancement

GOSAT was launched in January 2009 to monitor CO_2 column amounts from space (Yokota et al., 2009; Patra et al., 2021). The thermal and near-infrared sensor for carbon observation-Fourier-transform spectrometer (TANSO-FTS) onboard detects CO_2 columns by observing the short-wavelength infrared light reflected from Earth's surface under cloud-free conditions over land (Yokota et al., 2009). A series of XCO_2 datasets with different spatial and temporal resolutions were estimated from GOSAT using the global atmospheric transfer model (Kuze et al., 2016). Although we intended to estimate CO_2 emissions with the highest spatial and temporal resolutions, the level 2 CO_2 column amount, which provides measurements with a spatial resolution of 10.5 km at the subsatellite point, is too sparse for further analysis. A longer observation period will extend the coverage of satellite images, and temporal averaging will smooth out the short-term fluctuations.

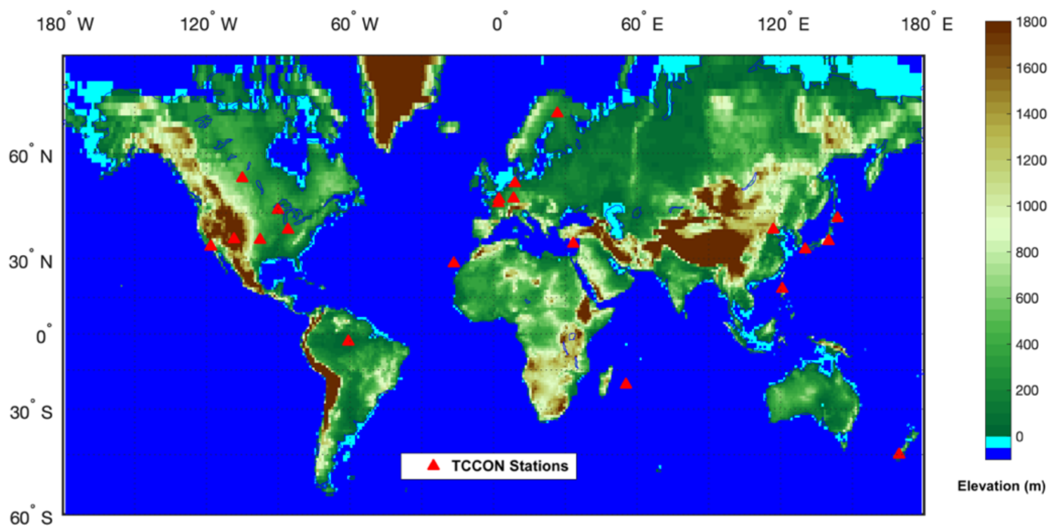

Figure 1. Distribution map of TCCON stations.

To identify the best temporal resolution that can accurately capture the variation trends while maintaining a high global coverage rate, the XCO_2 data obtained from the Total Carbon Column Observing Network (TCCON) were examined. The TCCON network observes multiple components with a high temporal resolution (Wunch et al., 2015). Because of its high precision, it has been widely adopted for validating satellite XCO_2 retrievals (Cogan et al., 2012; Zhang et al., 2017; Hong et al., 2022). The daily mean, daily median, 30-day moving average, and monthly mean of XCO_2 obtained in 2012–2020 at the Caltech station were analyzed. The daily data exhibited strong fluctuations, while seasonal variations were observed among all datasets. The 30-day moving average and monthly mean data reveal the seasonal cycle while smoothening the daily variations. Since the estimation method requires the XCO_2 products to be sampled as densely and frequently as possible, the

https://doi.org/10.5194/egusphere-2023-1347
Preprint. Discussion started: 30 August 2023
© Author(s) 2023. CC BY 4.0 License.

monthly GOSAT XCO_2 Level 3 product (FTS_C01S_3) with a spatial resolution of 2.5 × 2.5 degrees was employed to estimate CO_2 emissions.

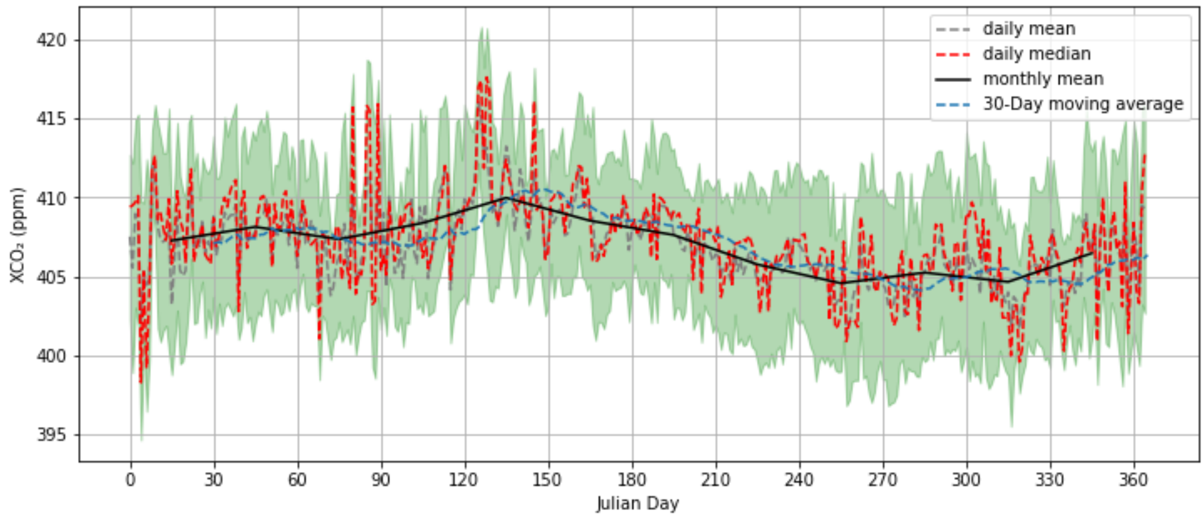

Figure 2. Daily mean, daily median, monthly mean, 30-day moving average of XCO_2 observed from the Caltech station from 2012 to 2020. The green-shaded area represents the σ on each day of a year.

The monthly mean XCO_2 data were calculated at the 24 stations within the TCCON network and employed as the ground truth to validate the GOSAT XCO_2 product. A good correlation between the GOSAT XCO_2 and the ground-based observation from TCCON, with a root mean square error of 1.564 ppm (Figure 3), proving that the satellite-derived XCO_2 data were accurate and could be used to estimate anthropogenic emissions.

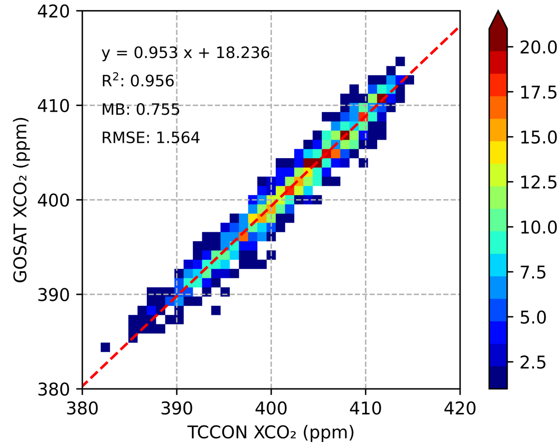

Figure 3. Comparison of monthly mean XCO_2 emissions obtained from GOSAT and its collocated TCCON stations in 2010–2019. The color bar denotes the sample size.

https://doi.org/10.5194/egusphere-2023-1347
Preprint. Discussion started: 30 August 2023
© Author(s) 2023. CC BY 4.0 License.

The overall variation in the atmospheric CO_2 column concentration was potentially influenced by anthropogenic emissions, long-range atmospheric transport, and natural fluxes. While anthropogenic CO_2 emissions only account for a small percentage of carbon fluxes (Streets et al., 2013), identifying the CO_2 fluxes arising from natural sources and anthropogenic emissions is critical. The monthly median from the sub-region was considered the background CO_2 fluxes and subtracted at each grid cell to isolate the anthropogenic emissions from CO_2 columns (Hakkarainen et al., 2016). Seven sub-regions were defined in this study according to their climatic characteristics and geographical locations: Tropical (23 °S–23 °N), North America (23 °N–60 °N, 180 °W–60 °W), Mediterranean (23 °N–60 °N, 0°–60 °E), East Asia (23 °N–60 °N, 60 °–180 °E), South America (23 °S–60 °S, 90 °W–30 °W), Africa (23 °S–60 °S, 0°–60 °E), and Oceania (23 °S–60 °S, 90 °E–180 °E). The XCO_2 anomaly (ΔXCO_2) was derived as follows:

$$\Delta XCO_2 = XCO_2(individual) - XCO_2(monthly\ median) \quad (1)$$

This step detrends the XCO_2 data while reducing the impact of potential regional-scale biases in the GOSAT product.

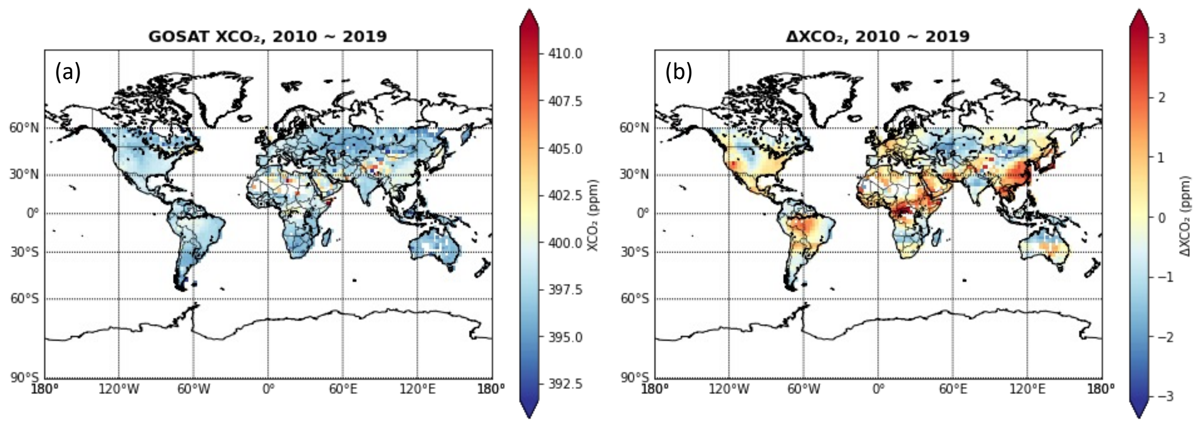

Figure 4. Distribution map of (a) the mean XCO_2 observed from the GOSAT project; (b) the mean of ΔXCO_2 observed from 2010 to 2019.

2.2 Ancillary data

In addition to the enhanced ΔXCO_2 from GOSAT, atmospheric conditions such as total column water vapor (tcwv), air temperature, local wind speed, and vertical velocity from ERA5 were also adopted as ancillary data (Table 1). The probability density function (PDF) of each input variable obtained from 2010 to 2019 on the global scale is provided in Figure 5. Although datasets with hourly and daily estimations were also available for ERA5, the analysis focused on monthly averaged data to align the reanalysis with the temporal resolution of the GOSAT product. To standardize the datasets obtained from multiple resources for further estimation, these data records were re-grided to a spatial resolution of 2.5 × 2.5 degrees.

https://doi.org/10.5194/egusphere-2023-1347
Preprint. Discussion started: 30 August 2023
© Author(s) 2023. CC BY 4.0 License.

Table 1. Summary of data characteristics on XCO_2 and ancillary data used in model development and validation analysis.

Data type	Data source	Description	Resolution
XCO_2	GOSAT	Averaged CO_2 dry air mole fraction unit: ppm	Monthly mean, 2.5 × 2.5 degrees
	TCCON	Averaged CO_2 dry air mole fraction unit: ppm	24 stations
ω500	ERA5	Vertical velocity at 500 hPa unit: hPa/day	Monthly mean, 0.25 × 0.25 degrees
Wind speed	ERA5	u-component of wind at 1000, 975, and 950 hPa unit: m/s	Monthly mean, 0.25 × 0.25 degrees
Air temperature	ERA5	Mean monthly near-surface temperature unit: °C	Monthly mean, 0.5 × 0.5 degrees
Total column water vapor	ERA5	Total column of vertically integrated water vapor unit: kg/m^2	Monthly mean, 0.25 × 0.25 degree
Carbon emissions	GFED	Monthly emissions from biomass burning unit: gC/m^2/month	Monthly mean, 0.25 × 0.25 degree
Anthropogenic emissions	ODIAC	CO_2 emissions from fossil fuel combustion, cement production, and gas flaring unit: gC/m^2/d	Monthly mean, 1 × 1 degree

ERA5 is the global climate and weather reanalysis developed by the European Centre for Medium-Range Weather Forecasts (ECMWF), and it integrates model simulations with observational data (Hersbach et al., 2020). Previous study has indicated that high wind speeds accelerate the spread of CO_2 thus weakening XCO_2 signals (Zheng et al., 2020). Therefore, the local wind field was used in the estimation process as an indicator of atmospheric movement in the horizontal direction in this study. The average wind speeds at 1000, 975, and 950 hPa were calculated to approximate the wind speed below 500 m (Beirle et al., 2011; Zheng et al., 2020). The positive value indicating air movement toward the east, and a negative value indicating air movement toward the west.

https://doi.org/10.5194/egusphere-2023-1347
Preprint. Discussion started: 30 August 2023
© Author(s) 2023. CC BY 4.0 License.

Large-scale atmospheric circulation is another driving force influencing regional changes in atmospheric concentration (Ma et al., 2018). Here the vertical velocity at 500 hPa (ω500) was utilized as the proxy of large-scale circulation (Bony et al., 2004). The negative values are related to convective motions, and the positive values are related to subsiding motions (Brogniez and Pierrehumbert, 2007). The ω500 peaked at 10 hPa/day, indicating that the large-scale movement was dominated by the Hadley subsidence.

The carbon emissions resulting from fires, obtained from the Global Fire Emissions Database (GFED), were also considered in the estimation process. This dataset was generated from MODIS (Moderate Resolution Imaging Spectroradiometer) direct broadcast burned-area products (Giglio et al., 2013; Shi et al., 2015; Jones et al., 2020). The monthly dataset at a spatial resolution of 0.25 × 0.25 degrees was adopted and re-grided for further analysis.

The bottom-up inventory of CO_2 emissions of ODIAC is a global high-resolution emissions data product for fossil fuel carbon dioxide emissions commonly adopted as reference data on CO_2 emissions (Oda et al., 2018). ODIAC combines the space-based nighttime light data and individual power plant emission/location profiles to estimate the global spatial extent of fossil fuel-related CO_2 emissions. It is used as a reference dataset for both model development and validation.

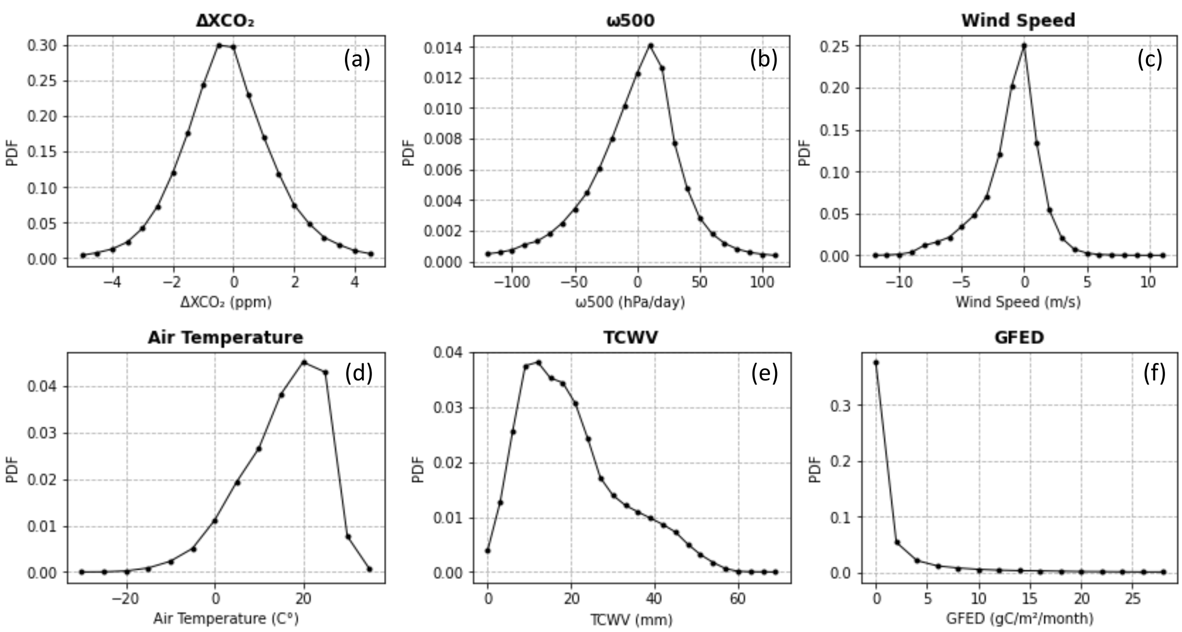

Figure 5. Normalized PDF for model inputs: (a) ΔXCO_2, (b) ω500, (c) wind speed, (d) air temperature, (e) tcwv, and (f) carbon emissions from fire in 2010–2019 on a global scale.

https://doi.org/10.5194/egusphere-2023-1347
Preprint. Discussion started: 30 August 2023
© Author(s) 2023. CC BY 4.0 License.

2.3 Dataset optimization

A total of 118,390 groups of samples were obtained for the period 2010 to 2019. The number of valid collocated data points obtained at each grid cell during the observation period is displayed in Figure 6. The data points were unevenly distributed across the globe. To accurately capture the spatial and temporal variations, grid cells with more than 84 measurements (representing 70% of the observation period) were further separated into training (~70%, 46,341 samples) and testing (~30%, 19,860 samples) subsets through the bootstrap resampling method. These subsets were utilized for model development and cross-validation, while the remaining grid cells were solely used for validation analysis. The aim of this resampling step was to collocate datasets into independent training and testing subsets while reducing the impact of the varying spatial distribution of the data points and the biases of satellite observation (Batista et al., 2004). Notably, none of the grid cells had more than 84 measurements in the high-latitude region; therefore, the emissions from this area were not considered.

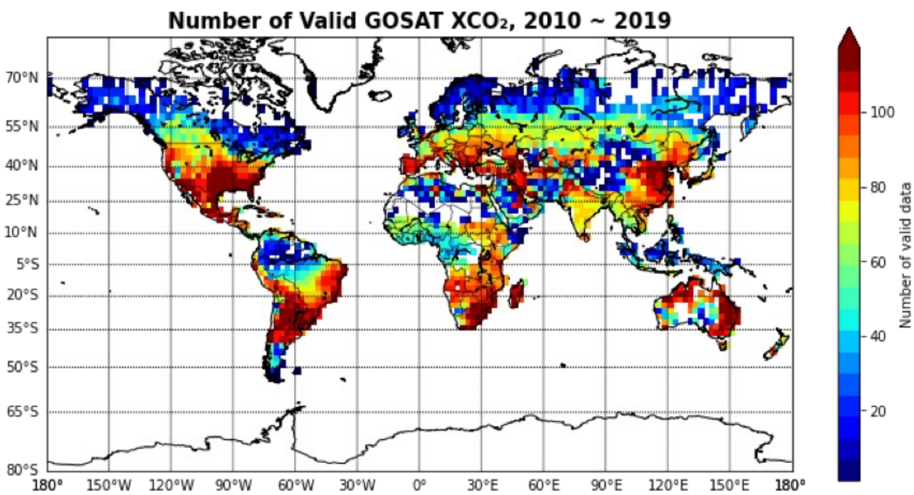

Figure 6. Number of valid GOSAT XCO_2 measurements in 2010–2019 in each grid cell. The color bar denotes the sample size.

3 Methodology

The core objective of this research was to accurately and directly estimate anthropogenic CO_2 emissions from enhanced satellite-based XCO_2 data using the GTWR model. Before the new model was developed, the XCO_2 data obtained from GOSAT were examined against ground-based measurements. ΔXCO_2 was extracted to enhance the emissions signals. Atmospheric transport is critical in estimating CO_2 emissions. Therefore, the atmospheric parameters, including atmospheric circulation in the horizontal and vertical directions, along with the near-surface air temperature and humidity information, should also be included as input variables in the estimation process. Additionally, ODIAC emissions data were employed as a

https://doi.org/10.5194/egusphere-2023-1347
Preprint. Discussion started: 30 August 2023
© Author(s) 2023. CC BY 4.0 License.

reference for CO_2 emissions for model development and validation analysis. As the research focused on global estimation, the considerable spatial and temporal variabilities in the relationship between ΔXCO_2 and CO_2 emissions were considered using the GTWR model. Grid cells with fewer than 70% valid measurements during the observation period (corresponding to ~84 measurements) could not sufficiently characterize the temporal variability. Therefore, only grid cells with more than 84 measurements were adopted for model training. Finally, the estimated results were validated against the ODIAC emissions dataset.

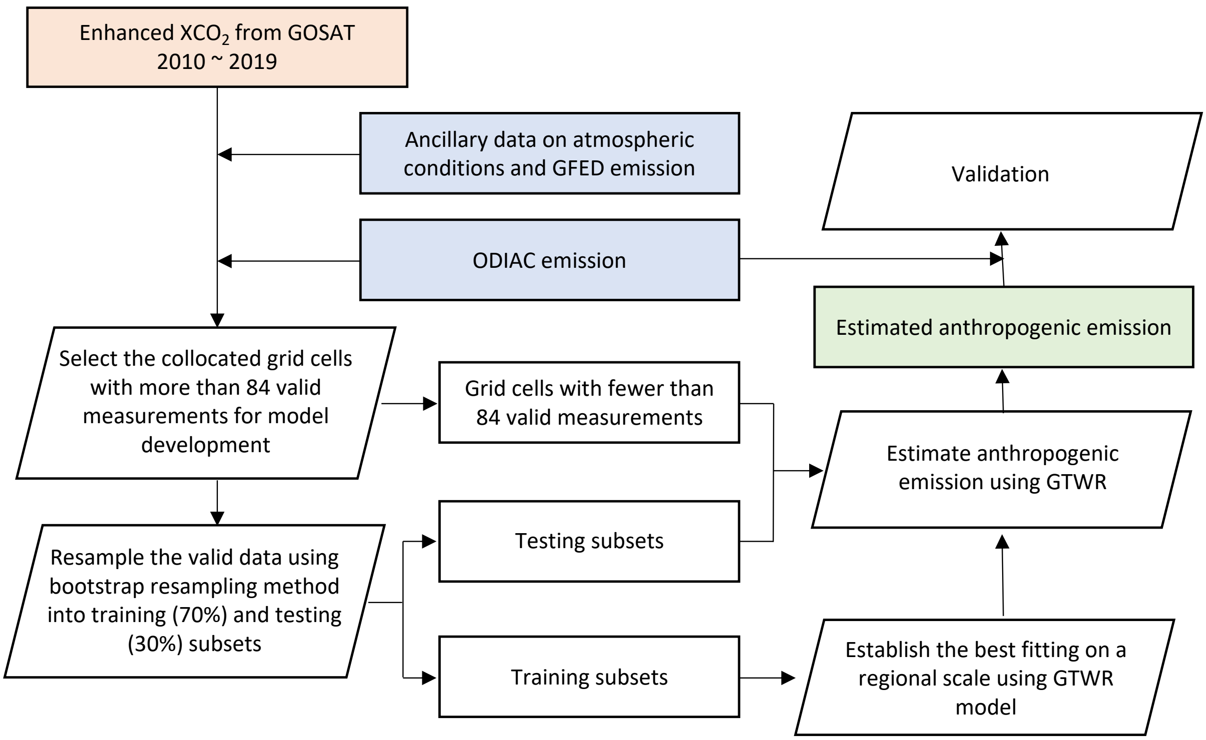

Figure 7. Flowchart of anthropogenic emissions estimation using ΔXCO_2 data obtained from GOSAT.

3.1 CO_2 emissions

The seasonality of variation trends, long atmospheric lifetime, and large variations in atmospheric background significantly complicate the measurement of anthropogenic CO_2 emissions (Streets et al., 2013; Hakkarainen et al., 2016; Pan et al., 2021). Here, ΔXCO_2 was calculated to enhance the emissions signals. To analyze the relationship between the CO_2 emissions and the input parameters, the composite of ODIAC emissions data were analyzed through the decomposition of the emissions data according to different intervals of the input variables. The mean of CO_2 emissions in a particular interval was analyzed, and the results revealed that the CO_2 emissions evolution was related to the atmospheric variables. A positive correlation existed between CO_2 emissions and ΔXCO_2 (Figure 8a), as the emissions increased with increasing ΔXCO_2. The inconsistent data

https://doi.org/10.5194/egusphere-2023-1347
Preprint. Discussion started: 30 August 2023
© Author(s) 2023. CC BY 4.0 License.

points for intervals with high ΔXCO_2 are possibly due to the limited number of measurements. Similar growth trends in CO_2 emissions were also observed for intervals of air temperature and tcwv, indicating a positive correlation between CO_2 emissions and the two atmospheric parameters. The decomposition of CO_2 emissions according to $\omega500$ showed that regions with a strong subsiding motion ($\omega500$ > 50 hPa/day) were associated with high CO_2 emissions. The areas with a weak subsiding motion associated with the low CO_2 emissions. Moreover, a negative correlation existed between CO_2 emissions and fire emissions.

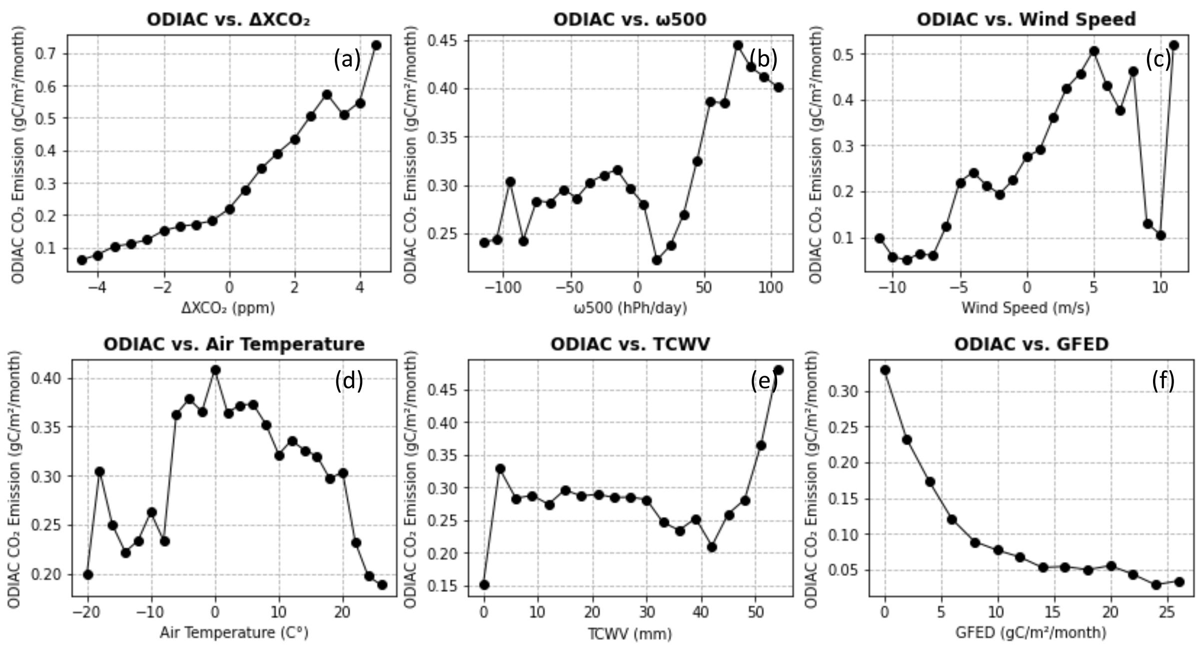

Figure 8: Composite CO_2 emissions under different atmospheric condition intervals: (a) ΔXCO_2 from GOSAT; (b) $\omega500$; (c) wind speed; (d) air temperature; (e) tcwv; (f) fire carbon emissions in 2010–2019 on a global scale.

3.2 GTWR model

The GTWR model was adopted to simulate the relationship between ΔXCO_2 and anthropogenic emissions with localized correction (Huang et al., 2010; He and Huang, 2018; Wu et al., 2021). This model captures spatiotemporal heterogeneity by incorporating a weighting matrix that considers both spatial and temporal dimensions. Because ΔXCO_2 is potentially an effect of human activities, long-range atmospheric transport, and natural fluxes, anthropogenic emissions can be expressed as follows:

https://doi.org/10.5194/egusphere-2023-1347
Preprint. Discussion started: 30 August 2023
© Author(s) 2023. CC BY 4.0 License.

$$AE_i = \beta_0(\mu_i, \nu_i, t_i) + \beta_1(\mu_i, \nu_i, t_i) \times \Delta XCO_{2_i} + \beta_2(\mu_i, \nu_i, t_i) \times \omega 500_i + \beta_3(\mu_i, \nu_i, t_i) \times WS_i + \beta_4(\mu_i, \nu_i, t_i) \times AT_i + \beta_5(\mu_i, \nu_i, t_i) \times TCWV_i + \beta_6(\mu_i, \nu_i, t_i) \times FE_i + \varepsilon_i \quad (2)$$

where AE_i are the monthly anthropogenic emissions of sample i at location (μ_i, ν_i) at time t_i. β_0 is the intercept at location (μ_i, ν_i) at time t_i. $\beta_1 - \beta_6$ denote the location-and-time-specific slopes for ΔXCO_2 observed from GOSAT, ω500, wind speed (*WS*), air temperature (*AT*), total column water vapor (*TCWV*), and fire emissions (*FE*), respectively, and ε_i represents the offset. The detailed statistics on the input variables for model development for each sub-region are presented in Table 2.

Table 2. Statistics of the input variables for model development for each sub-region.

Sub-region		Input parameters					
		ΔXCO_2 (ppm)	ω500 (hPa/day)	WS (m/s)	AT (° C)	TCWV (kg/m^2)	FE (gC/m^2/month)
Tropical (13,826)	Max	6.65	265.63	9.56	34.80	65.04	191.97
	Min	−7.45	−340.13	−10.92	3.45	1.73	0.00
	Mean	−0.37	4.06	−1.76	23.47	27.81	5.53
North America (8,243)	Max	6.02	699.26	6.09	34.55	53.58	340.95
	Min	−4.59	−355.47	−8.70	−9.70	3.30	0.00
	Mean	0.24	4.75	0.14	16.05	18.66	1.72
Mediterranean (7,128)	Max	6.25	649.94	9.33	38.80	39.01	27.21
	Min	−7.75	−385.73	−9.12	−11.75	3.03	0.00
	Mean	−0.05	4.30	−0.16	16.06	16.26	0.91
East Asia (8,683)	Max	8.66	747.07	8.64	35.75	70.84	81.95
	Min	−6.13	−358.13	−8.49	−22.90	0.72	0.00
	Mean	0.64	9.91	−0.15	13.36	18.46	1.23
South America (4,120)	Max	3.86	1466.46	7.70	29.90	52.09	228.27
	Min	−3.65	−1101.55	−7.41	−3.90	0.78	0.00
	Mean	0.12	10.94	−0.95	16.91	20.71	1.41
Africa (1,874)	Max	2.69	252.71	3.26	29.45	47.51	89.21
	Min	−2.83	−148.27	−8.05	6.35	4.17	0.00
	Mean	−0.02	4.51	−0.59	19.31	17.47	2.00
Oceania (2,467)	Max	3.34	649.28	6.71	33.75	45.09	1115.40
	Min	−4.13	−248.97	−8.95	−1.10	5.19	0.01
	Mean	−0.06	21.67	−0.91	18.64	18.70	4.72

https://doi.org/10.5194/egusphere-2023-1347
Preprint. Discussion started: 30 August 2023
© Author(s) 2023. CC BY 4.0 License.

4 Results

4.1 Validation of CO_2 emissions

The monthly anthropogenic emissions were estimated with the GTWR model using the ΔXCO_2 extracted from GOSAT XCO_2 data and the corresponding atmospheric information. To analyze the differences between the two data records, the mean bias (MB) was calculated:

$$MB = \frac{1}{n}\sum_{i=1}^{n}(AE_{predicted} - AE_{ODIAC}) \quad (2)$$

where n denotes the sample size, $AE_{predicted}$ denotes the anthropogenic emissions obtained from the GOSAT product, and AE_{ODIAC} denotes the reference data on CO_2 emissions obtained from ODIAC.

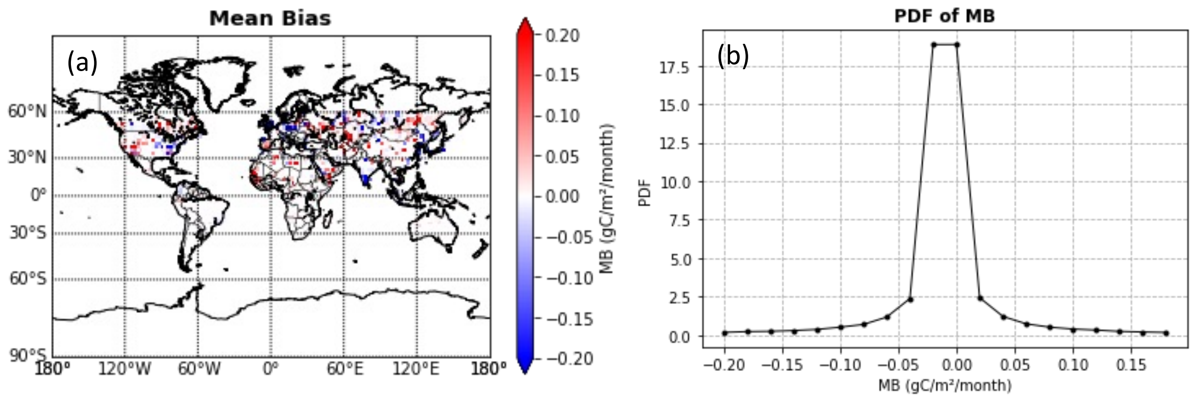

Figure 9: Distribution map of (a) the MB between anthropogenic emissions estimated using satellite-based measurement and the reference ODIAC data; (b) the PDF of the MB.

The distribution map of the MB on CO_2 emissions measured from 2010 to 2019 is presented in Figure 9. The spatially changing patterns of the emissions data estimated from satellite-based XCO_2 measurements are similar to the ODIAC product. Underestimation was observed in East China, South India, the British Isles, Germany, and the eastern United States, where high-emission regions are located. Despite the differences between the two datasets, the majority of the MBs between the two data records were within ±0.05 $gC/m^2/month$, demonstrating the robust accuracy of the model on a global scale.

To further evaluate the performance of the newly derived satellite-based CO_2 emissions dataset, the coefficient of determination (R^2) was calculated as follows:

https://doi.org/10.5194/egusphere-2023-1347
Preprint. Discussion started: 30 August 2023
© Author(s) 2023. CC BY 4.0 License.

$$R^2 = \left[\frac{\sum_{i=1}^{n}(AE_{ODIAC} - \overline{AE_{ODIAC}})(AE_{Predicted} - \overline{AE_{Predicted}})}{\sqrt{\sum_{i=1}^{n}(AE_{ODIAC} - \overline{AE_{ODIAC}})^2(AE_{Predicted} - \overline{AE_{Predicted}})^2}}\right]^2 \tag{3}$$

where $\overline{AE_{ODIAC}}$ and $\overline{AE_{Predicted}}$ denote the average values of anthropogenic emissions from ODIAC and the satellite-based measurements, respectively. The overall verification for the training dataset and the validation for the testing dataset are shown in Figure 10. High correlations existed between the satellite-derived emissions and the ODIAC reference data, with R^2 of 0.951 and 0.929 for the training and testing subsets, respectively.

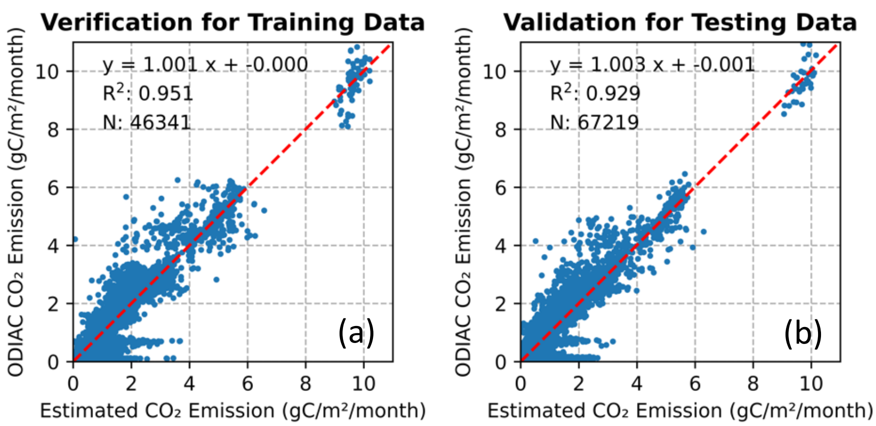

Figure 10: Scatter plot of anthropogenic emissions estimated from GOSAT and the collocated ODIAC product from 2010 to 2019 for (a) the training dataset and (b) the testing dataset.

4.2 Variations in CO_2 emissions

The characteristics of global emissions were investigated using the CO_2 emissions data. The annual mean of CO_2 emissions was calculated, and the interannual variation (ΔCO_2) was obtained as follows:

$$\Delta CO_2(grid, t) = AE_{(grid,t)} - AE_{(grid,t-1)} \tag{4}$$

where $\Delta CO_2(grid, t)$ indicates the interannual variation of anthropogenic emissions for each grid in year *t*. $AE_{(grid,t)}$ and $AE_{(grid,t-1)}$ denote the anthropogenic emission at each grid in year *t* and the year before, respectively.

The distribution maps of the mean ΔCO_2 obtained from the newly derived emissions data from the GOSAT and ODIAC products in 2010–2019 are displayed in Figure 11. Positive values indicate an increasing trend in CO_2 emissions, while negative values indicate a decreasing trend. As shown in the figure, most areas maintained a steady emissions rate. Although some discrepancies exist between the two datasets, both records show an increasing trend in emissions in Canada, Colombia, several

https://doi.org/10.5194/egusphere-2023-1347
Preprint. Discussion started: 30 August 2023
© Author(s) 2023. CC BY 4.0 License.

West African countries, northern Europe, India, and China during the observation period, while emissions in the United States decreased over time from 2010 to 2019.

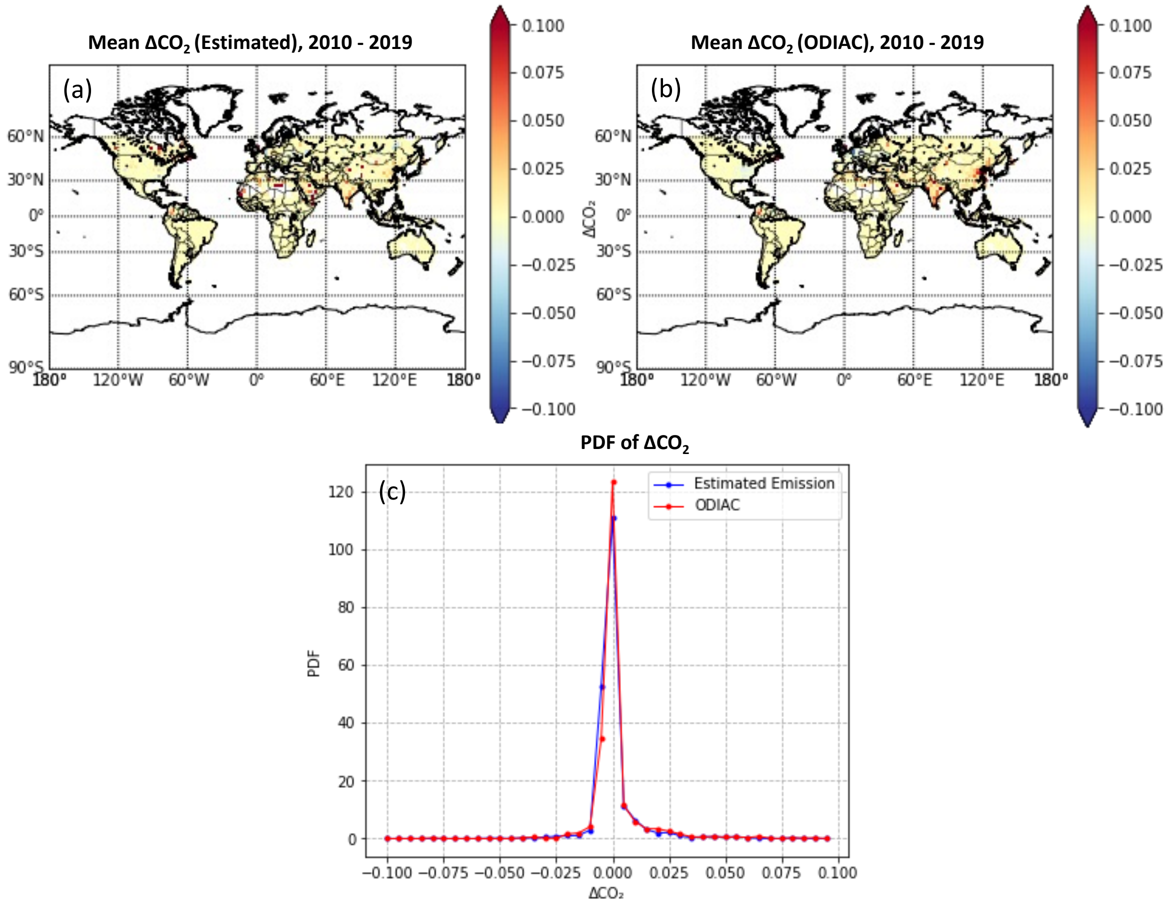

Figure 11: (a) Distribution map of the mean ΔCO_2 from anthropogenic emissions estimated from the satellite-based measurement from GOSAT in 2010–2019; (b) mean ΔCO_2 from ODIAC; (c) the PDF of ΔCO_2 of the estimated data.

230 The PDFs of ΔCO_2 for the two data records are displayed in Figure 11(c). Although most areas maintained a steady emissions rate during the observation period, many areas exhibited a decrease in CO_2 emissions over time. The good agreement between the two data records demonstrates the applicability of the newly derived data record for observing the variability of CO_2 emissions on a global scale.

https://doi.org/10.5194/egusphere-2023-1347
Preprint. Discussion started: 30 August 2023
© Author(s) 2023. CC BY 4.0 License.

5 Conclusions

Accurate and reliable statistics on anthropogenic CO_2 emissions are critical for evaluating mitigation progress. Unlike the conventional method that calculates emissions using "bottom-up" inventories, the estimation of anthropogenic emissions from satellites is a data-driven approach that provides an independent measurement of carbon emissions. The XCO_2 retrieved from GOSAT, the atmospheric information (including ω500, wind speed, air temperature, and tcwv), and the fire emissions data from GFED were employed as input parameters for the model development. The GTWR model, which accounts for spatial and temporal variations in data through a spatiotemporal weighting mechanism, was applied to estimate anthropogenic emissions from satellite-based measurements. Moreover, the bootstrap resampling method was employed to reduce the potential impacts of the varying spatial distribution of the data points and the effects of the biases of satellite retrieval.

The newly derived anthropogenic CO_2 emissions dataset from the enhanced XCO_2 measurements revealed the variation trend of CO_2 emissions on a global scale. The emissions data were validated against the ODIAC product, and the satellite-derived data strongly agreed with the reference data, with an R^2 of 0.929. The majority of the MBs on a global scale were within ±0.05 gC/m^2/month, demonstrating the spatial independence of the model on a global scale. The agreement in characteristics observed between the estimated results and ODIAC demonstrates the applicability of the newly estimated data record for observing the variability of CO_2 emissions on a global scale.

In summary, this study demonstrated a feasible method for accurately estimating CO_2 emissions from satellite-derived CO_2 column amounts. The validation results showed that the CO_2 emissions estimated using the GTWR model were robust both spatially and temporally on a global scale. The findings have significant implications for applications involving the use of CO_2 satellite data to independently monitor CO_2 emissions at different scales. Although characterizing atmospheric dynamics solely based on the above model inputs could be considered a simplification, the atmospheric parameters considered in our approach can serve as a meaningful proxy for atmospheric conditions, making our approach easily applicable on a global scale. Satellite images with finer spatiotemporal resolution will provide more information in the future.

Author contributions. BH and JH designed the research. JH carried out the data analysis and prepared all the figures. JH and BH contributed to the interpretation of the results and wrote the paper.

Competing interests. The authors do not declare any competing interests.

Acknowledgements. This work was supported by the National Key Research and Development Program of China (2022YFB3903700 and 2019YFC1510400), the Research Grants Council of Hong Kong (AoE/E-603/18), and the National Natural Science Foundation of China (No. 42271439), and Dazuyunfeng Data Collection Project (Grant No.D.01.18.00901). The XCO_2 data were obtained from the GOSAT Project (ftp://gosat-ds.eo.esa.int/) operated by the National Institute for Environmental Studies (NIES). The ancillary data on atmospheric conditions were obtained from the European Centre for

© Author(s) 2023. CC BY 4.0 License.

Medium-Range Weather Forecasts (ECMWF) ERA5 reanalysis products (https://cds.climate.copernicus.eu). The fire emissions data were obtained from the global fire emissions database (https://www.geo.vu.nl/~gwerf/GFED/GFED4/). The ODIAC CO_2 emissions data (https://db.cger.nies.go.jp/dataset/ODIAC/DL_odiac2020b.html) were provided by the Center for Global Environmental Research at NIES, and the column-averaged amount of CO_2 was provided by the Total Carbon Column Observing Network hosted by CaltechDATA (https://tccondata.org/). Professional English language editing support provided by AsiaEdit (aisaedit.com).

References

Batista, G. E. A. P. A., Prati, R. C., and Monard, M. C.: A Study of the Behavior of Several Methods for Balancing Machine Learning Training Data, SIGKDD Explor Newsl, 6, 20–29, https://doi.org/10.1145/1007730.1007735, 2004.

Beirle, S., Boersma, K. F., Platt, U., Lawrence, M. G., and Wagner, T.: Megacity Emissions and Lifetimes of Nitrogen Oxides Probed from Space, Science, 333, 1737–1739, https://doi.org/10.1126/science.1207824, 2011.

Bony, S., Dufresne, J.-L., Le Treut, H., Morcrette, J.-J., and Senior, C.: On dynamic and thermodynamic components of cloud changes, Clim. Dyn., 22, 71–86, https://doi.org/10.1007/s00382-003-0369-6, 2004.

Brogniez, H. and Pierrehumbert, R. T.: Intercomparison of tropical tropospheric humidity in GCMs with AMSU-B water vapor data, Geophys. Res. Lett., 34, https://doi.org/10.1029/2006GL029118, 2007.

Cogan, A. J., Boesch, H., Parker, R. J., Feng, L., Palmer, P. I., Blavier, J.-F. L., Deutscher, N. M., Macatangay, R., Notholt, J., Roehl, C., Warneke, T., and Wunch, D.: Atmospheric carbon dioxide retrieved from the Greenhouse gases Observing SATellite (GOSAT): Comparison with ground-based TCCON observations and GEOS-Chem model calculations, J. Geophys. Res. Atmospheres, 117, https://doi.org/10.1029/2012JD018087, 2012.

Crippa, M., Guizzardi, D., Banja, M., Solazzo, E., Muntean, M., Schaaf, E., Pagani F, Monforti-Ferrario, F., Olivier, J. G. J., Quadrelli, R., Risquez Martin, A., Taghavi-Moharamli, P., Grassi, G., Rossi, S., Oom, D., Branco, A., San-Miguel, J., and Vignati, E.: CO2 emissions of all world countries: JRC/IEA/PBL 2022 report, Publications Office of the European Union, LU, 2022.

Crowell, S., Baker, D., Schuh, A., Basu, S., Jacobson, A. R., Chevallier, F., Liu, J., Deng, F., Feng, L., McKain, K., Chatterjee, A., Miller, J. B., Stephens, B. B., Eldering, A., Crisp, D., Schimel, D., Nassar, R., O'Dell, C. W., Oda, T., Sweeney, C., Palmer, P. I., and Jones, D. B. A.: The 2015–2016 carbon cycle as seen from OCO-2 and the global in situ network, Atmospheric Chem. Phys., 19, 9797–9831, https://doi.org/10.5194/acp-19-9797-2019, 2019.

Friedlingstein, P., Jones, M. W., O'Sullivan, M., Andrew, R. M., Hauck, J., Peters, G. P., Peters, W., Pongratz, J., Sitch, S., Le Quéré, C., Bakker, D. C. E., Canadell, J. G., Ciais, P., Jackson, R. B., Anthoni, P., Barbero, L., Bastos, A., Bastrikov, V., Becker, M., Bopp, L., Buitenhuis, E., Chandra, N., Chevallier, F., Chini, L. P., Currie, K. I., Feely, R. A., Gehlen, M., Gilfillan, D., Gkritzalis, T., Goll, D. S., Gruber, N., Gutekunst, S., Harris, I., Haverd, V., Houghton, R. A., Hurtt, G., Ilyina, T., Jain, A. K., Joetzjer, E., Kaplan, J. O., Kato, E., Klein Goldewijk, K., Korsbakken, J. I., Landschützer, P., Lauvset, S. K., Lefèvre, N., Lenton, A., Lienert, S., Lombardozzi, D., Marland, G., McGuire, P. C., Melton, J. R., Metzl, N., Munro, D. R., Nabel, J. E. M. S., Nakaoka, S.-I., Neill, C., Omar, A. M., Ono, T., Peregon, A., Pierrot, D., Poulter, B., Rehder, G., Resplandy, L., Robertson, E., Rödenbeck, C., Séférian, R., Schwinger, J., Smith, N., Tans, P. P., Tian, H., Tilbrook, B., Tubiello, F. N., van der Werf, G. R., Wiltshire, A. J., and Zaehle, S.: Global Carbon Budget 2019, Earth Syst. Sci. Data, 11, 1783–1838, https://doi.org/10.5194/essd-11-1783-2019, 2019.

Friedlingstein, P., Jones, M. W., O'Sullivan, M., Andrew, R. M., Bakker, D. C. E., Hauck, J., Le Quéré, C., Peters, G. P., Peters, W., Pongratz, J., Sitch, S., Canadell, J. G., Ciais, P., Jackson, R. B., Alin, S. R., Anthoni, P., Bates, N. R., Becker, M., Bellouin, N., Bopp, L., Chau, T. T. T., Chevallier, F., Chini, L. P., Cronin, M., Currie, K. I., Decharme, B., Djeutchouang, L., Dou, X., Evans, W., Feely, R. A., Feng, L., Gasser, T., Gilfillan, D., Gkritzalis, T., Grassi, G., Gregor, L., Gruber, N., Gürses, Ö., Harris, I., Houghton, R. A., Hurtt, G. C., Iida, Y., Ilyina, T., Luijkx, I. T., Jain, A. K., Jones, S. D., Kato, E., Kennedy, D., Klein Goldewijk, K., Knauer, J., Korsbakken, J. I., Körtzinger, A., Landschützer, P., Lauvset, S. K., Lefèvre, N., Lienert, S., Liu, J., Marland, G., McGuire, P. C., Melton, J. R., Munro, D. R., Nabel, J. E. M. S., Nakaoka, S.-I., Niwa, Y., Ono, T., Pierrot, D., Poulter, B., Rehder, G., Resplandy, L., Robertson, E., Rödenbeck, C., Rosan, T. M., Schwinger, J., Schwingshackl, C., Séférian, R., Sutton, A. J., Sweeney, C., Tanhua, T., Tans, P. P., Tian, H., Tilbrook, B., Tubiello, F., van der Werf, G., Vuichard, N., Wada, C., Wanninkhof, R., Watson, A., Willis, D., Wiltshire, A. J., Yuan, W., Yue, C., Yue, X., Zaehle, S., and Zeng, J.: Global Carbon Budget 2021, Earth Syst. Sci. Data Discuss., 1–191, https://doi.org/10.5194/essd-2021-386, 2021.

Giglio, L., Randerson, J. T., and van der Werf, G. R.: Analysis of daily, monthly, and annual burned area using the fourth-generation global fire emissions database (GFED4), J. Geophys. Res. Biogeosciences, 118, 317–328, https://doi.org/10.1002/jgrg.20042, 2013.

Hakkarainen, J., Ialongo, I., and Tamminen, J.: Direct space-based observations of anthropogenic CO2 emission areas from OCO-2, Geophys. Res. Lett., 43, 11,400-11,406, https://doi.org/10.1002/2016GL070885, 2016.

He, Q. and Huang, B.: Satellite-based high-resolution PM2.5 estimation over the Beijing-Tianjin-Hebei region of China using an improved geographically and temporally weighted regression model, Environ. Pollut., 236, 1027–1037, https://doi.org/10.1016/j.envpol.2018.01.053, 2018.

Hersbach, H., Bell, B., Berrisford, P., Hirahara, S., Horányi, A., Muñoz-Sabater, J., Nicolas, J., Peubey, C., Radu, R., Schepers, D., Simmons, A., Soci, C., Abdalla, S., Abellan, X., Balsamo, G., Bechtold, P., Biavati, G., Bidlot, J., Bonavita, M., Chiara, G. D., Dahlgren, P., Dee, D., Diamantakis, M., Dragani, R., Flemming, J., Forbes, R., Fuentes, M., Geer, A., Haimberger, L., Healy, S., Hogan, R. J., Hólm, E., Janisková, M., Keeley, S., Laloyaux, P., Lopez, P., Lupu, C., Radnoti, G., Rosnay, P. de, Rozum, I., Vamborg, F., Villaume, S., and Thépaut, J.-N.: The ERA5 global reanalysis, Q. J. R. Meteorol. Soc., 146, 1999–2049, https://doi.org/10.1002/qj.3803, 2020.

Hong, X., Zhang, P., Bi, Y., Liu, C., Sun, Y., Wang, W., Chen, Z., Yin, H., Zhang, C., Tian, Y., and Liu, J.: Retrieval of Global Carbon Dioxide From TanSat Satellite and Comprehensive Validation With TCCON Measurements and Satellite Observations, IEEE Trans. Geosci. Remote Sens., 60, 1–16, https://doi.org/10.1109/TGRS.2021.3066623, 2022.

Huang, B., Wu, B., and Barry, M.: Geographically and temporally weighted regression for modeling spatio-temporal variation in house prices, Int. J. Geogr. Inf. Sci., 24, 383–401, https://doi.org/10.1080/13658810802672469, 2010.

Jones, M. O., Running, S. W., Kimball, J. S., Robinson, N. P., and Allred, B. W.: Terrestrial primary productivity indicators for inclusion in the National Climate Indicators System, Clim. Change, 163, 1855–1868, https://doi.org/10.1007/s10584-018-2155-9, 2020.

Kuze, A., Suto, H., Shiomi, K., Kawakami, S., Tanaka, M., Ueda, Y., Deguchi, A., Yoshida, J., Yamamoto, Y., Kataoka, F., Taylor, T. E., and Buijs, H. L.: Update on GOSAT TANSO-FTS performance, operations, and data products after more than 6 years in space, Atmospheric Meas. Tech., 9, 2445–2461, https://doi.org/10.5194/amt-9-2445-2016, 2016.

Le Quéré, C., Jackson, R. B., Jones, M. W., Smith, A. J. P., Abernethy, S., Andrew, R. M., De-Gol, A. J., Willis, D. R., Shan, Y., Canadell, J. G., Friedlingstein, P., Creutzig, F., and Peters, G. P.: Temporary reduction in daily global CO2 emissions during the COVID-19 forced confinement, Nat. Clim. Change, 10, 647–653, https://doi.org/10.1038/s41558-020-0797-x, 2020.

Liu, Z., Ciais, P., Deng, Z., Lei, R., Davis, S. J., Feng, S., Zheng, B., Cui, D., Dou, X., Zhu, B., Guo, R., Ke, P., Sun, T., Lu, C., He, P., Wang, Y., Yue, X., Wang, Y., Lei, Y., Zhou, H., Cai, Z., Wu, Y., Guo, R., Han, T., Xue, J., Boucher, O., Boucher, E., Chevallier, F., Tanaka, K., Wei, Y., Zhong, H., Kang, C., Zhang, N., Chen, B., Xi, F., Liu, M., Bréon, F.-M., Lu, Y., Zhang, Q., Guan, D., Gong, P., Kammen, D. M., He, K., and Schellnhuber, H. J.: Near-real-time monitoring of global CO2 emissions reveals the effects of the COVID-19 pandemic, Nat. Commun., 11, 5172, https://doi.org/10.1038/s41467-020-18922-7, 2020.

Ma, J., Chadwick, R., Seo, K.-H., Dong, C., Huang, G., Foltz, G. R., and Jiang, J. H.: Responses of the Tropical Atmospheric Circulation to Climate Change and Connection to the Hydrological Cycle, Annu. Rev. Earth Planet. Sci., 46, 549–580, https://doi.org/10.1146/annurev-earth-082517-010102, 2018.

Oda, T. and Maksyutov, S.: A very high-resolution (1 km×1 km) global fossil fuel CO_2 emission inventory derived using a point source database and satellite observations of nighttime lights, Atmospheric Chem. Phys., 11, 543–556, https://doi.org/10.5194/acp-11-543-2011, 2011.

Oda, T., Maksyutov, S., and Andres, R. J.: The Open-source Data Inventory for Anthropogenic CO_2, version 2016 (ODIAC2016): a global monthly fossil fuel CO_2 gridded emissions data product for tracer transport simulations and surface flux inversions, Earth Syst. Sci. Data, 10, 87–107, https://doi.org/10.5194/essd-10-87-2018, 2018.

Olivier, J. G. J., Van Aardenne, J. A., Dentener, F. J., Pagliari, V., Ganzeveld, L. N., and Peters, J. A. H. W.: Recent trends in global greenhouse gas emissions:regional trends 1970–2000 and spatial distributionof key sources in 2000, Environ. Sci., 2, 81–99, https://doi.org/10.1080/15693430500400345, 2005.

O'Neill, B. C., Liddle, B., Jiang, L., Smith, K. R., Pachauri, S., Dalton, M., and Fuchs, R.: Demographic change and carbon dioxide emissions, The Lancet, 380, 157–164, https://doi.org/10.1016/S0140-6736(12)60958-1, 2012.

Pachauri, R. K., Mayer, L., and Intergovernmental Panel on Climate Change (Eds.): Climate change 2014: synthesis report, Intergovernmental Panel on Climate Change, Geneva, Switzerland, 151 pp., 2015.

Pan, G., Xu, Y., and Huang, B.: Evaluating national and subnational CO2 mitigation goals in China's thirteenth five-year plan from satellite observations, Environ. Int., 156, 106771, https://doi.org/10.1016/j.envint.2021.106771, 2021.

Patra, P. K., Hajima, T., Saito, R., Chandra, N., Yoshida, Y., Ichii, K., Kawamiya, M., Kondo, M., Ito, A., and Crisp, D.: Evaluation of earth system model and atmospheric inversion using total column CO2 observations from GOSAT and OCO-2, Prog. Earth Planet. Sci., 8, 25, https://doi.org/10.1186/s40645-021-00420-z, 2021.

Schneising, O., Buchwitz, M., Reuter, M., Heymann, J., Bovensmann, H., and Burrows, J. P.: Long-term analysis of carbon dioxide and methane column-averaged mole fractions retrieved from SCIAMACHY, Atmospheric Chem. Phys., 11, 2863–2880, https://doi.org/10.5194/acp-11-2863-2011, 2011.

Shi, Y., Matsunaga, T., Saito, M., Yamaguchi, Y., and Chen, X.: Comparison of global inventories of CO2 emissions from biomass burning during 2002–2011 derived from multiple satellite products, Environ. Pollut., 206, 479–487, https://doi.org/10.1016/j.envpol.2015.08.009, 2015.

Solomon, S., Intergovernmental Panel on Climate Change, and Intergovernmental Panel on Climate Change (Eds.): Climate change 2007: the physical science basis: contribution of Working Group I to the Fourth Assessment Report of the Intergovernmental Panel on Climate Change, Cambridge University Press, Cambridge ; New York, 996 pp., 2007.

Solomon, S., Plattner, G.-K., Knutti, R., and Friedlingstein, P.: Irreversible climate change due to carbon dioxide emissions, Proc. Natl. Acad. Sci., 106, 1704–1709, https://doi.org/10.1073/pnas.0812721106, 2009.

https://doi.org/10.5194/egusphere-2023-1347
Preprint. Discussion started: 30 August 2023
© Author(s) 2023. CC BY 4.0 License.

Streets, D. G., Canty, T., Carmichael, G. R., de Foy, B., Dickerson, R. R., Duncan, B. N., Edwards, D. P., Haynes, J. A., Henze, D. K., Houyoux, M. R., Jacob, D. J., Krotkov, N. A., Lamsal, L. N., Liu, Y., Lu, Z., Martin, R. V., Pfister, G. G., Pinder, R. W., Salawitch, R. J., and Wecht, K. J.: Emissions estimation from satellite retrievals: A review of current capability, Atmos. Environ., 77, 1011–1042, https://doi.org/10.1016/j.atmosenv.2013.05.051, 2013.

Wu, S., Huang, B., Wang, J., He, L., Wang, Z., Yan, Z., Lao, X., Zhang, F., Liu, R., and Du, Z.: Spatiotemporal mapping and assessment of daily ground NO2 concentrations in China using high-resolution TROPOMI retrievals, Environ. Pollut., 273, 116456, https://doi.org/10.1016/j.envpol.2021.116456, 2021.

Wunch, D., Toon, G. C., Sherlock, V., Deutscher, N. M., Liu, C., Feist, D. G., and Wennberg, P. O.: The Total Carbon Column Observing Network's GGG2014 Data Version, 42, 2015.

Xu, Y.: Environmental Policy and Air Pollution in China: Governance and Strategy (Edition 1), Routledge, https://doi.org/10.4324/9780429452154, 2020.

Yang, D., Liu, Y., Feng, L., Wang, J., Yao, L., Cai, Z., Zhu, S., Lu, N., and Lyu, D.: The First Global Carbon Dioxide Flux Map Derived from TanSat Measurements, Adv. Atmospheric Sci., 38, 1433–1443, https://doi.org/10.1007/s00376-021-1179-7, 2021.

Yang, S., Lei, L., Zeng, Z., He, Z., and Zhong, H.: An Assessment of Anthropogenic CO2 Emissions by Satellite-Based Observations in China, Sensors, 19, 1118, https://doi.org/10.3390/s19051118, 2019.

Yokota, T., Yoshida, Y., Eguchi, N., Ota, Y., Tanaka, T., Watanabe, H., and Maksyutov, S.: Global Concentrations of CO₂ and CH₄ Retrieved from GOSAT: First Preliminary Results, Sola, 5, 160–163, https://doi.org/10.2151/sola.2009-041, 2009.

Zhang, L. L., Yue, T. X., Wilson, J. P., Zhao, N., Zhao, Y. P., Du, Z. P., and Liu, Y.: A comparison of satellite observations with the XCO2 surface obtained by fusing TCCON measurements and GEOS-Chem model outputs, Sci. Total Environ., 601–602, 1575–1590, https://doi.org/10.1016/j.scitotenv.2017.06.018, 2017.

Zheng, B., Chevallier, F., Ciais, P., Broquet, G., Wang, Y., Lian, J., and Zhao, Y.: Observing carbon dioxide emissions over China's cities and industrial areas with the Orbiting Carbon Observatory-2, Atmospheric Chem. Phys., 20, 8501–8510, https://doi.org/10.5194/acp-20-8501-2020, 2020.